Ligand binding strength explains the distribution of iron in the North Atlantic Ocean

Anh L. D. Pham[1] **and Takamitsu Ito**[1]

[1]School of Earth and Atmospheric Sciences, Georgia Institute of Technology, Atlanta Georgia U.S.A.

Key Points:

- Hypotheses explaining the pattern of dissolved iron in the subtropical North Atlantic are tested in an ocean biogeochemistry model
- Increasing the rate of biological uptake makes a negligible impact on the modeled iron distribution
- Increasing the scavenging rate or decreasing the ligand binding strength can explain the observed iron pattern, but the latter mechanism is better supported by observations

Corresponding author: Anh L. D. Pham, anh.pham@eas.gatech.edu

Abstract
Observations of dissolved iron (dFe) in the subtropical North Atlantic revealed remarkable features: while the near-surface dFe concentration is low despite receiving high dust deposition, the subsurface dFe concentration is high. We test several hypotheses that might explain this feature in an ocean biogeochemistry model with a refined Fe cycling scheme. These hypotheses invoke a stronger lithogenic scavenging rate, rapid biological uptake, and a weaker binding between Fe and a ubiquitous, refractory ligand. While the standard model overestimates the surface dFe concentration, a 10-time stronger biological uptake run causes a slight reduction in the model surface dFe. A 10-fold decrease in the binding strength of the refractory ligand, suggested by recent observations, starts reproducing the observed dFe pattern, with a potential impact for the global nutrient distribution. An extreme value for the lithogenic scavenging rate can also match the model dFe with observations, but this process is still poorly constrained.

1 Introduction

Iron (Fe) is a crucial element in the marine ecosystem and biogeochemistry because it is one of the limiting nutrients for the phytoplankton growth [*Boyd and Ellwood*, 2010; *Moore et al.*, 2013]. The GEOTRACES program is rapidly expanding the data coverage for the global Fe distribution over the last decade [*Mawji et al.*, 2015; *Schlitzer et al.*, 2018], which provides an excellent opportunity to advance our understanding of the ocean Fe cycling. One region of special interest is the oligotrophic subtropical North Atlantic, where the concentrations of dissolved and particulate Fe and their isotopic compositions are measured along the zonal (GA03) and meridional (GA03e) transects by the USGT10 and USGT11 cruises [*Boyle et al.*, 2015; *Fitzsimmons et al.*, 2015; *Hatta et al.*, 2015; *Conway and John*, 2014]. In this region, the biological productivity is considered to be less sensitive to Fe than to macronutrients [*Moore et al.*, 2013]. However, several observational and experimental studies showed that the availability of Fe here can limit the growth of nitrogen-fixing cyanobacteria and the phosphate acquisition by microbial community [*Browning et al.*, 2017; *Moore et al.*, 2006, 2009]. In addition, this region has a dynamic Fe cycling with multiple Fe supplies from both internal cycling and external inputs [*Hatta et al.*, 2015; *Conway and John*, 2014]. Moreover, globally significant water masses are formed in the North Atlantic, and their preformed dissolved Fe (dFe) can influence the far field via long-range transports [*Conway et al.*, 2018]. It is thus important to understand processes controlling the dFe distribution in this region.

The zonal and meridional GA03 transects reveal a unique feature of the dFe pattern in the subtropical North Atlantic. Despite receiving high dFe input from the atmospheric deposition, the surface dFe concentration is relatively low (0.3 - 0.5 nM) (Fig. 1bc). In contrast, 9 out of 13 current ocean general circulation and biogeochemistry models (OGCBMs) compiled by *Tagliabue et al.* [2016] have a relatively high surface dFe concentration (~1-2 nM) Furthermore, the observed subsurface dFe maximum (1.4 - 1.6 nM) (Fig. 1bc) are underestimated by 7 of 13 models included in *Tagliabue et al.* [2016]. These models encapsulate our mechanistic understanding of the Fe cycling through parameterizations of relevant biochemical processes, thus these biases indicate gaps in our understanding.

Several hypotheses have been suggested to explain this unique feature and resolve the systematic model biases. First, a recent model study suggested a stronger scavenging by lithogenic particles as a possible mechanism to decrease the surface dFe where dust deposition is high [*Ye and Völker*, 2017]. Second, the Fe uptake rate of phytoplankton can significantly increase under the high dust plume to rapidly consume dFe. *Twining and Baines* [2013] and *Twining et al.* [2015] showed a 3-fold higher for Fe quota in the North Atlantic cells, compared with those measured in the Pacific and Southern Oceans. However, the efficiency of these two mechanisms depends on the concentration and binding strength of organic ligands due to their dFe protection against removal processes [*Tagliabue et al.*, 2017].

Ye and Völker [2017] pointed out that if their model uses a dynamic ligand scheme instead of a globally uniform ligand concentration of 1nM, it requires a greater lithogenic scavenging rate in order to bring the model surface dFe concentration closer to observations. While there has been significant advances in our understanding of ligands thanks to the expanding GEOTRACES dataset and experimental studies [*Buck et al.*, 2015; *Gerringa et al.*, 2016; *Boiteau and Repeta*, 2015], there still is a significant uncertainty in the ligand sources, sinks, and binding strength with free Fe [*Hassler et al.*, 2017]. This leads to uncertainties on the relative importance of retention and removal processes in regulating the dFe distribution in the subtropical North Atlantic and how these processes might change in the future [*Hutchins and Boyd*, 2016; *Tagliabue et al.*, 2016].

The objective of this study is to explore which mechanism would best explain the Fe distribution in the subtropical North Atlantic by performing a suite of sensitivity experiments in an OGCBM. Specifically, we purposefully alter different aspects of the model Fe parameter in each experiment and analyze the resulting dFe pattern. The model includes all major processes controlling the ocean Fe cycling such as dFe inputs from atmospheric dust, bottom sediment and hydrothermal sources, dFe scavenging onto and release from lithogenic and organic particles, and dFe retention by spatially-varying ligands. The development of this model is documented in a recent publication, which shows major improvements in the large-scale ocean dFe distribution [*Pham and Ito*, 2018].

2 Model configuration and experimental design

2.1 Model configuration

The ocean biogeochemistry model used in this study is essentially the same as the model used in our recent study [*Pham and Ito*, 2018], which is based on the Massachusetts Institute of Technology general circulation model (MITgcm) [*Marshall et al.*, 1997a,b]. The ocean bathymetry is configured in a 1°x 1°horizontal resolution and 23 non-uniform vertical levels with the vertical grid ranging from 10m in the surface to 500m in the deep ocean. Mesoscale eddies are parameterized by the isopycnal tracer and thickness diffusion scheme [*Solomon*, 1971; *Redi*, 1982; *Gent and Mcwilliams*, 1990] and the mixed-layer processes are parameterized by the K-Profile Parameterization scheme [*Large et al.*, 1994]. The model is run offline, using climatological monthly circulation fields obtained from the Estimating the Circulation and Climate of the Ocean (ECCO) version 3 [*Wunsch and Heimbach*, 2007]. The biogeochemical aspect of the model is mostly the same as in *Pham and Ito* [2018], which carries 6 tracers; dissolved inorganic carbon (DIC), alkalinity, phosphate (PO_4^{3-}), dissolved organic phosphorus (DOP), dFe, and oxygen (O_2). Biological production is modulated by the availability of nutrients (PO_4^{3-} and dFe) and light through Monod function.

As in *Pham and Ito* [2018], we consider three external supplies for dFe: atmospheric deposition, continental shelves, and hydrothermal vents. In this model, the biological Fe:P uptake ratio changes as a function of the dFe concentration, which aim to represent the luxury Fe uptake of diatoms such as in the subarctic Pacific and the Southern Ocean [*Ingall et al.*, 2013]. The majority of dFe is bound to ligands and is protected from being removed by scavenging and precipitation [*Rue and Bruland*, 1995]. The new feature of our model is its ability to include multiple classes of ligands with different spatial patterns and binding strengths [*Pham and Ito*, 2018]. This model represents three ligand classes. L_1 is assumed to be the biologically produced siderophores with relatively high binding strength [*Adly et al.*, 2015; *Macrellis et al.*, 2001]. This is parameterized as a linear function of the DOP concentration in the model, $L_1 = \alpha[DOP]$, and is given the strongest conditional stability constant of $K_{L1} = 10^{12}\ L/mol$. L_2 is essentially the dissolved organic matter produced from the remineralization of particulate organic matter [*Laglera and van den Berg*, 2009; *Velasquez et al.*, 2016; *Vraspir and Butler*, 2009]. This component is parameterized as a linear function of the Apparent Oxygen Utilization (AOU), $L_2 = \beta AOU$, and its binding strength is set to $K_{L2} = 10^{11}\ L/mol$. The new feature of this work is the inclusion of the third class (L_3), represent-

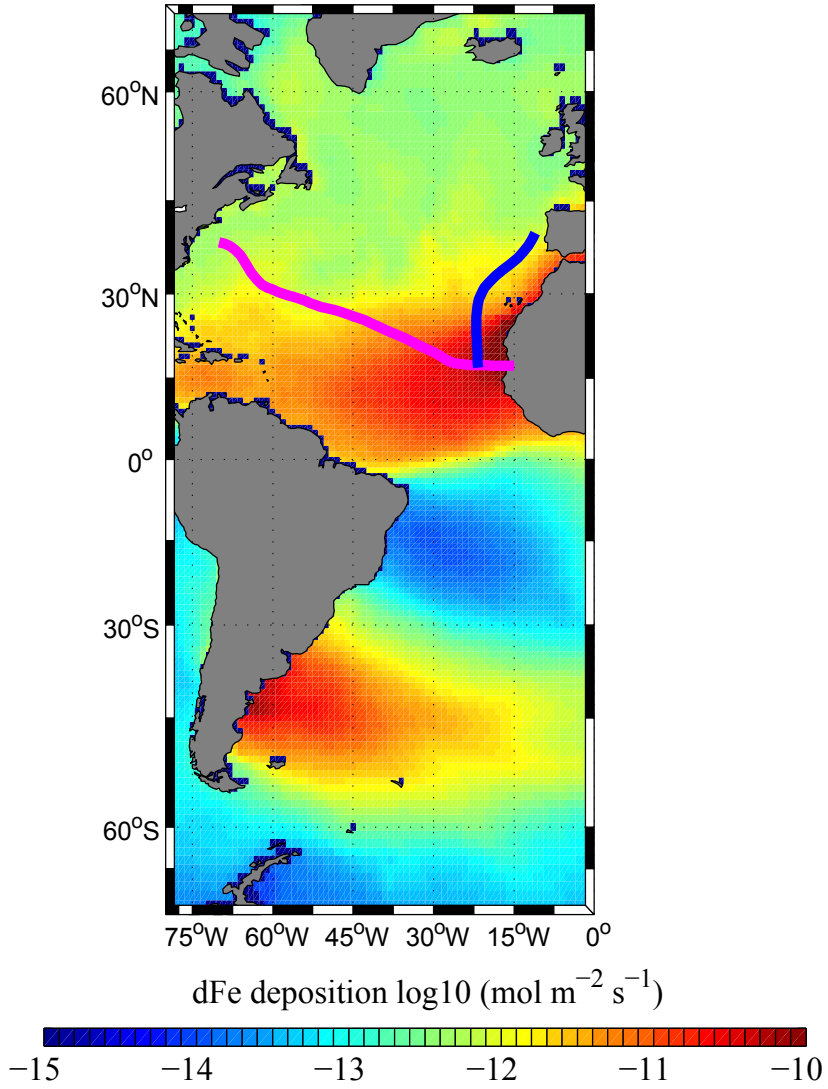

Figure 1. Atmospheric dFe deposition over the Atlantic Ocean used in this study. Blue and magenta lines indicate the tracks of the meridional GA03e and zonal GA03 cruises from GEOTRACES program, respectively.

ing the refractory dissolve organic carbon (DOC) as a background component with a uniform concentration, $L_3 = L_{refract}$ [*Hassler et al.*, 2011]. Following *Pham and Ito* [2018], the empirical constants in this ligand parameterization are calibrated to fit the observed ligand distribution in the least squares sense ($\alpha = 6.1 \cdot 10^{-5}$, $\beta = 1.3 \cdot 10^{-5}$), and $L_{refract} = 1.3nM$. There is uncertainty in the binding strength of the refractory, humic-like L_3, as several studies reported to be weaker than 10^{11} L/mol [*Gledhill and Buck*, 2012], thus we vary the magnitude of K_{L3} between 10^{11} and 10^{10} L/mol in the sensitivity experiments. The two-class parameterization of *Pham and Ito* [2018] is essentially the same as setting $K_{L3} = K_{L2} = 10^{11}$ L/mol, so a decreased retention of dFe is anticipated if we use $K_{L3} < 10^{11}$ L/mol.

dFe not bound to ligands (free Fe, $[Fe']$) can be removed from the water column by scavenging onto lithogenic and organic particles, based on a first-order bulk scavenging rate, and by precipitation [*Pham and Ito*, 2018]. While the organic scavenging process is parameterized as a function of particulate organic matter concentration [*Parekh et al.*, 2005], the lithogenic scavenging is parameterized as a first order loss process [*Pham and Ito*, 2018; *Galbraith et al.*, 2010] with a rate coefficient: K_{inorg}:

$$Fe_{scav}^{inorg} = K_{inorg}[Fe'] \tag{1}$$

The scavenging of $[Fe']$ through this process can enhance under the high dust plume when lithogenic particle concentration increases [*Ye and Völker*, 2017; *Ye et al.*, 2011]. To represent this effect, the inorganic scavenging rate is scaled by the atmospheric dust deposition (JFe_{dust}) as follows:

$$K_{inorg} = K_{inorg0} \left(\frac{JFe_{dust}}{\langle JFe_{dust} \rangle} \right)^n \tag{2}$$

where the reference scavenging coefficient, K_{inorg0}, is the same as in *Pham and Ito* [2018] (set to $2.0 \times 10^{-7} s^{-1}$), JFe_{dust} is the atmospheric dFe dust flux at each model grid cell in the surface ocean, and $\langle JFe_{dust} \rangle$ is the global mean dust Fe flux. Thus, K_{inorg} can vary spatially in the surface water as a function of the atmospheric dFe flux, but its value below the surface is still set to K_{inorg0}. In addition, the minimum value for K_{inorg} is also be set as K_{inorg0}, keeping it from being extremely low under the regions of low dust deposition such as the Southern Ocean. The exponent n for the dust-flux dependence is set to 1 for the control simulation following [*Pham and Ito*, 2018], but it is varied in the sensitivity run. The scavenged Fe can be released back to the water by remineralization and desorption [*Pham and Ito*, 2018]. [Fe'] can also be lost through precipitation [*Fitzsimmons et al.*, 2015], parameterized in the model following the approach by *Pham and Ito* [2018]. dFe loss through colloidal pumping process [*Honeyman and Santschi*, 1989; *Tagliabue et al.*, 2016] is not yet resolved in our model.

2.2 Experimental design

First, the model was integrated for 1,000 years with a standard parameterization (*Control* run) to reach a quasi-steady state. Five additional experiments were then started from the end of the *control* run with perturbed parameterizations, and were further run for 1,000 years to achieve new quasi-steady states. These experiments aim to evaluate the roles of various processes controlling the ocean dFe cycling in the subtropical North Atlantic. Model experiments are setup as follows:

- "*Control*" run applies the ligand and scavenging parameterizations as in *Pham and Ito* [2018]; ($K_{L3} = 10^{11} L/mol$, $n = 1$)
- "*Stronger scav.*" run allows a stronger inorganic scavenging rate in the surface water under the high dust deposition; ($K_{L3} = 10^{11} L/mol$, $n = 1.5$)
- "*Stronger uptake*" run has the same setup as the *Control* run but with a 10 times bigger biological uptake ratio between Fe and phosphorus (P)
- "*Weaker L3*" run sets a weaker binding strength for L_3; ($K_{L3} = 10^{10} L/mol$, $n = 1$)

- "*Stronger scav. + weaker L3*" run is the combination of the *Weaker L3* run and *Stronger scav.* runs; ($K_{L3} = 10^{10} L/mol$, $n = 1.5$)
- " *Stronger scav. 2*" run allows a stronger inorganic scavenging rate under the high dust deposition for the whole euphotic layer (0-200m); ($K_{L3} = 10^{11} L/mol$, $n = 1.5$)

The second and fourth runs examine the relative roles of ligand and scavenging in modulating the subtropical North Atlantic Fe cycling. The effect of increasing the power-law dependence (n) in the second and sixth experiments roughly translates to a 1000-fold increase in the net scavenging rate relative to the reference value (K_{inorg0}) under the high dust plume. The difference between these two runs is that the *Stronger scav. 2* allows the increase in inorganic scavenging rate not just only at the surface water but also throughout the surface water column (200m). These experiments explore the uncertainty regarding the impact of a potentially high lithogenic scavenging rate on the upper ocean dFe distribution in the subtropical North Atlantic. The *Stronger uptake* run investigates the uncertainty associated with the Fe-P uptake ratio of phytoplankton, as reported by a wide range for this value in *Twining and Baines* [2013]. *Twining et al.* [2015] shows a 3-fold higher for Fe quota in the North Atlantic cells, compared with those measured in the Pacific and Southern Ocean, which may have an impact on the surface dFe concentration in this region.

3 Mechanisms controlling the dFe distribution in the subtropical North Atlantic

Our model-data comparison is focused in the upper 1,000m, thus we zoom in the depth from 0 - 1,000m in Figs. 2 and 3 and compress the rest of the water column. In addition, the pattern correlations between model runs and observations and mean model biases are calculated for the surface (0-250m), subsurface (250-1000m), and the upper 1,000m waters (Table S1).

The *control* run reproduces some features of the subsurface dFe maximum signals observed in both the western and eastern margins, which are formed by remineralization and/or by the dFe release from the adjacent reduced sediments [*Hatta et al.*, 2015]. However, as is the case with most models included in *Tagliabue et al.* [2016], it overestimates the surface dFe concentration by ~0.7 - 0.8 nM and underestimates the vertical and horizontal extent of the mid-depth dFe maximum in the eastern margin (Figs 2a and 3a). This leads to a model subsurface dFe maximum shallower than observed. The strong dFe gradients around 200m - 600m from 60 - 40°W (Fig 2a) and near the surface from 30 - 40°N (Fig 3a) are not reproduced in the model because the dFe concentration there is higher than observed. Thus, the pattern correlations between the *control* run and observations are low (0.44 and 0.54 for the upper 1000m water column of the GA03e and GA03 transects, respectively) and the mean model biases are generally positive (0.15 and 0.26) (Table S1). Our model is also not able to reproduce the high dFe hydrothermal level observed at 3,000-4,000m from 50 - 40°W.

A stronger inorganic scavenging rate in the surface water (*stronger scav.* run) slightly decreases the surface dFe concentration in both transects by ~0.3 nM (Figs 2c and 3c), moderately increasing the pattern correlations with observations for the upper 1,000m water column relative to the control run (from 0.44 to 0.55 and from 0.54 to 0.66 - Table S1). The mean model biases in the upper 1,000m also decrease as more dFe is scavenged by lithogenic particles. However, the subsurface (200-1,000m) dFe maximum in the eastern margin is still shallower than observed. Observed subsurface dFe gradients in the central subtropical gyre (around 40°W in Fig 2c) and in the eastern subtropics (around 30°N in Fig 3c) are still not reproduced.

Allowing the inorganic scavenging rate to be increased from 0-200m under the high dust plume (*Stronger scav. 2* run) significantly decreases the dFe concentration in the surface water by more than 1 nM (Fig. S1). The mean model biases are significantly decreased in the upper 1000m to negative values (Table S1). However, the subsurface dFe maximum in the eastern margin also decreases by more than 1 nM and further underestimates the ob-

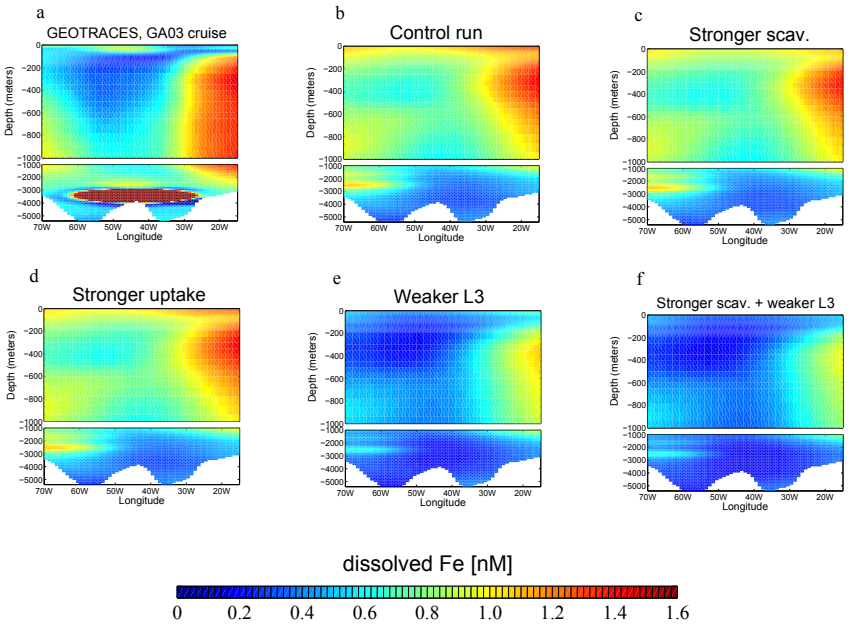

Figure 2. dFe distribution along the zonal GA03 transect: (a) *Observations*, (b) *Control* run, (c) *Stronger scav.* run, (d) *Stronger uptake* (e) *Weaker L3* run, and (f) *Stronger scav.* + *weaker L3* run . White color indicates the topography.

served subsurface dFe concentration, even though it starts to appear in a deeper level than the *control* run. Overall, the model thermocline dFe concentration in this run underestimates the observations, except for the extreme dFe signal around 800-1000m in the western margin (Fig. S1). The diminishing subsurface dFe is caused by the intense inorganic scavenging in this run, reducing the transport of dFe from the surface to subsurface waters. In contrast, the model subsurface dFe maximum in the western margin seems to overestimate observations, implying different formation mechanisms. The high level of dFe here might be formed via the subsurface dFe supply from continental shelves [*Hatta et al.*, 2015], thus not being affected by the reduction of dFe transport from the surface. The pattern correlation with the observation is 0.1 and is much lower than the control run (Table S1) due to a greater misfit in the subsurface dFe concentration. The result of this sensitivity run implies that an extremely high scavenging rate in the upper water column could eventually bring the model surface dFe concentration down to the observed level but at the expense of further decreasing the model subsurface dFe.

The *stronger uptake* run applies a ten times higher value for the Fe-P uptake ratio (R_{FeP}), but its effect on the surface dFe concentration seems to be relatively minor when compared with the *control* run (Figs 2d and 3d). This experiment is intended to assess the ecosystem response to the high dust deposition by allowing a higher rate of dFe uptake under the dust plume. In our model, the biological productivity in the oligotrophic subtropical North Atlantic region is low due to the macronutrients limitation [*Moore et al.*, 2013]. Therefore, an increase in the uptake Fe-P ratio in this particular model did not show a major shift in the regional biological activity and dFe distribution. It is beyond the scope of this study to examine the response of nitrogen-fixing bacteria in the large and episodic dust dFe deposition [*Moore et al.*, 2009], which requires an explicit ecosystem component. The mean model biases slightly increase in this run (Table S1), which may be caused by a higher R_{FeP}

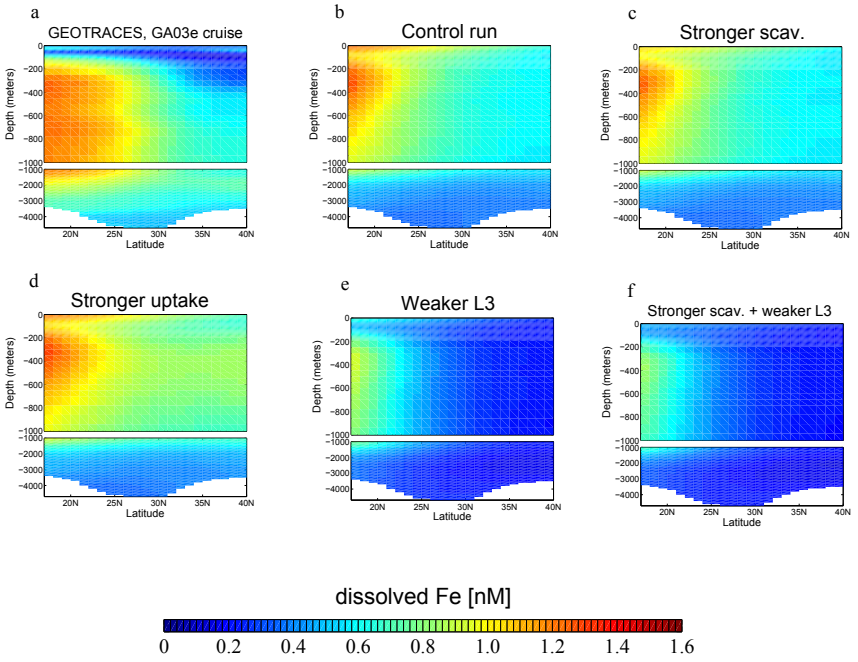

Figure 3. dFe distribution along the meridional GA03e transect: (a) *Control* run, (b) *Stronger scav.* run, (c)*Weaker L3* run, and (d) *Stronger scav.* + *weaker L3* run

ratio of remineralization and subsequent retention of the remineralized Fe by the subsurface ligands.

The *weaker L3* run shows significant improvements. It significantly decreases the surface dFe (~0.8 nM) and deepens the subsurface dFe maximum (Figs 2e and 3e). When the binding strength of L_3 is decreased, dust-deposited dFe is more effectively scavenged onto sinking organic particles, which then release dFe back at mid-depth waters via remineralization. Thus, lowering the binding strength of L_3 is an effective mechanism not only in reducing the model surface dFe concentration but also in redistributing the model dFe into the thermocline. This model run also reproduces the strong dFe gradients around 200m - 600m around 40°W (Fig 2e) and near the surface water around 30°N (Fig 3e). The pattern correlations between the model and observation are greatly improved from the control run (improving from 0.44 to 0.72 for the meridional GA03e transect and from 0.54 to 0.89 for the zonal GA03 - see Table S1). The mean model biases also shift to underestimation of the upper 1,000m water (-0.25 for GA03e and -0.19 for GA03). However, the thermocline (200-1,000m) dFe concentration is decreased in magnitude, especially in the western margin. As discussed above, the high level of dFe in the western margin is likely to be formed by the dFe sedimentary source, not by the redistributing of dust-deposited Fe between the surface and subsurface waters as in the eastern margin.

We further examine underlying mechanisms behind changes in the sensitivity runs by analyzing changes in the average dFe removal fluxes of each sensitivity run relative to the *Control* from 0-100m along 30°-15°W, 15°-25°N. Figure 5 shows 4 groups of bar chart for 4 model scenarios with each color representing different terms in the dFe removal fluxes. In the *Strongscav1* run, the inorganic scavenging increases by $\sim 0.18\ nM/year$ (light blue) relative to the *Control* at the expense of decreasing the other sink terms, especially the organic scavenging (dark blue). Lower concentration of dFe reduces the biological consump-

tion (brown) and the production of particulate organic Fe (dark blue), leading to a modest decrease of the surface dFe concentration in this run. It is possible to significantly decrease the surface dFe by further increasing inorganic scavenging rate (*Strong scav. 2* run). Similar to the previous run, the other removal fluxes partially compensate the increased scraveng-ing loss due to the decreased availability of dFe and biological production, but the inorganic scavenging flux is significantly increased ($\sim 0.4\ nM/year$) and dominates the dFe balance. As a result, it causes a large decrease in the surface dFe concentration, but it also reduces the transport of dust-deposited dFe from the surface to subsurface waters, leading to underesti-mation of the subsurface dFe concentration. In the *Strong uptake* run, the biological uptake increases by less than 0.1 $nM/year$ (brown bar), and changes in the other fluxes are even smaller. The impact of increasing biological uptake is insignificant due to the macro-nutrient limitation in this region. In the *Weaker L3* run, the total removal flux is similar to the *Strong scav. 2* (2.9 vs. 2.8 $nM/year$). However, the underlying mechanisms for increasing dFe re-moval fluxes are different. While the decrease of surface dFe in the *Strong scav.2* run relies solely on inorganic scavenging, the *Weaker L3* run decreases ligand binding strength, thereby enhancing both organic and inorganic scavenging fluxes. The difference in organic scaveng-ing flux ($\sim +0.15 nM/year$) between *Weaker L3* and *Strong scav.2* enhances the downward transport of dFe through remineralization, thus improving the model dFe distribution in the thermocline.

Combination of both mechanisms (stronger inorganic scavenging at the surface + weaker L_3) further decreases the surface dFe concentration (Figs 2f and 3f). The eastern subsurface dFe maximum also seems to be further decreased. While the mean bias (underestimation) is slightly enhanced (Table S1), there is little change in the pattern of the dFe distribution be-tween this run and the *weaker L3* run. Indeed, the pattern correlations between model and observations are essentially the same between these two runs. Comparison of all the sensitiv-ity runs in Figs 2, 3, and S1 suggests that weakening the binding strength of L_3 is the mech-anism that best explains dFe pattern in the subtropical North Atlantic and reduces model bi-ases.

4 Discussion and Conclusion

The improved spatial coverage and quality of Fe data provides a unique opportunity to evaluate our understanding of the ocean Fe cycling [*Mawji et al.*, 2015; *Schlitzer et al.*, 2018]. This study focused on the subtropical North Atlantic Ocean, where current OGCBMs have difficulty reproducing the observations [*Tagliabue et al.*, 2016]. This is an important region for studying the ocean Fe cycling because of its diverse dFe sources and sinks, and the complex internal cycling of dFe within the water column [*Hatta et al.*, 2015; *Conway et al.*, 2018]. Moreover, the dFe cycling in this region can have a far-reaching impact on the global marine biogeochemistry and ecosystems because of the forming of deep water masses that transport preformed Fe to far-field regions and because of its control on the growth of nitrogen-fixing bacteria. Since the subtropical North Atlantic receives high dust deposition [*Conway and John*, 2014], many models included in *Tagliabue et al.* [2016] show a relatively high surface dFe concentration of 1 - 2 nM. In contrast, the observed surface dFe is relatively low with a magnitude of 0.3 - 0.5 nM [*Hatta et al.*, 2015]. On the one hand, this indicates that these models underestimate the near-surface dFe sink including scavenging and/or bio-logical uptake. On the other hand, the degree to which these mechanisms can decrease the surface dFe depends on the concentration and binding strength of ligands, which are still un-certain [*Hassler et al.*, 2017; *Gledhill and Buck*, 2012]. This study examines mechanism be-hind the observed dFe patterns in the subtropical North Atlantic through model experiments in an OGCBM with an improved Fe cycling scheme [*Pham and Ito*, 2018].

The sensitivity run with a 10 times higher value for the biological uptake ratio R_{FeP} only has a negligible impact on the 0-1,000m dFe pattern due to the macronutrient-limited biological production in this region. A sensitivity run with a stronger lithogenic scaveng-ing rate lowers the surface dFe concentration but it causes a significant negative bias in the

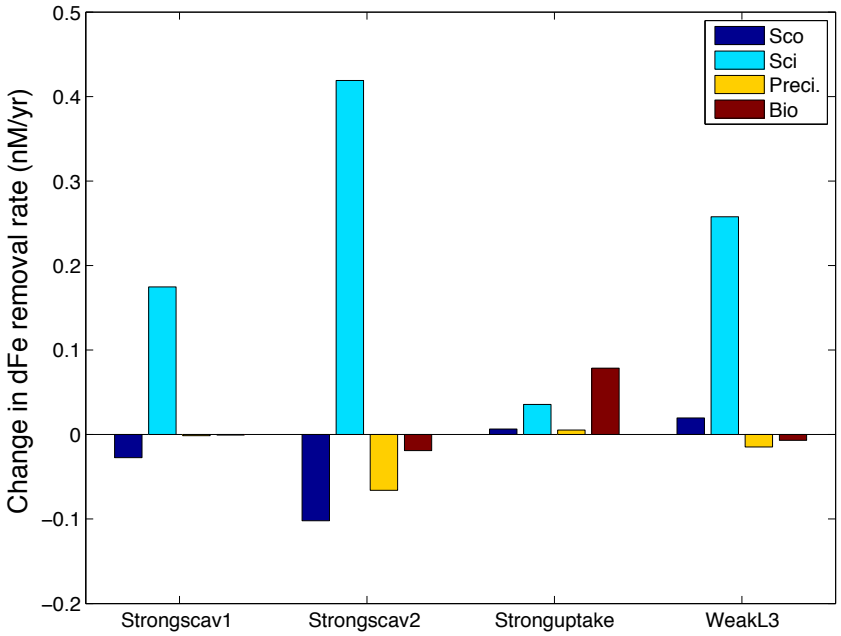

Figure 4. Changes in the average dFe removal fluxes ($nM/year$) from 0-100m along 30°-15°W, 15°-25°N for each sensitivity run relative to the control run. The dark blue, light blue, yellow, and brown bars indicate the removal fluxes from (Sco) organic scavenging, (Sci) inorganic scavenging, (Preci) precipitation, and (Bio) biological uptake, respectively.

thermocline dFe concentration. In contrast, a sensitivity run with a 10 times weaker refractory ligand class significantly reduces the model surface dFe while sustaining the subsurface dFe maximum at a similar level to observations by increasing the release of scavenged Fe in the thermocline. This leads to a significant improvement in the pattern correlation between model and observations.

The observed ligand data has been greatly expanded over the last few years thanks to the GEOTRACES program [*Buck et al.*, 2015; *Gerringa et al.*, 2015; *Buck et al.*, 2018]. Several modeling studies have taken advantage of these data to develop a dynamic ligand scheme in OGCBMs, which could significantly improve the model ligand and dFe representations [*Völker and Tagliabue*, 2015]. However, given a large uncertainty in the ligand binding strength, those models still represent only one ligand class, which is considered to be the most dominant and has the binding strength of $10^{11} L/mol$ [*Ye and Völker*, 2017; *Völker and Tagliabue*, 2015]. Our results argue for the inclusion of different ligand classes, each with distinct sources and binding strength. Representing the refractory ligand L_3 with a weak binding strength of $10^{10} L/mol$ significantly improved our model in the subtropical North Atlantic. Our results are thus in line with a recent review on the ligand classification, which suggests a ligand spectrum of three groups [*Hassler et al.*, 2017]. In addition, the modeled binding strength of L_3 (K = $10^{10} L/mol$) is consistent with the measurement of *Buck et al.* [2015] for the weakest ligand class along the GA03 transect. Nevertheless, our simple ligand parameterization should be considered as only a first step towards a mechanistic ligand model, which should dynamically represent a continuum of ligand classes, rather than a few discrete ones. The long-lived refractory-DOC ligand class can be a crucial factor for the Fe cycling in the subtropical North Atlantic, where ligand sources from microbial activity and remineralization are limited due to the low biological production [*Buck et al.*, 2015]. Given the ubiquitous and longevity of this ligand class, its binding strength and concentration could have an important impact on the global Fe distribution, especially for the Fe-depleted surface waters. Strong lithogenic scavenging and high biological Fe uptake could also play some roles but their effects are likely confined within regions of high dust deposition.

Acknowledgments
AP and TI are grateful for funding support from the National Science Foundation (OCE-1737188, OPP-1744755). Two anonymous reviewers provided helpful comments. The model result files are available at: https://github.com/anhlpham/PhamItoGRL2018. The model source code and input forcing files are stored at: http://shadow.eas.gatech.edu/ Ito/webdata/data.html. Observational data of dissolved iron is publicly accessible in the GEOTRACES website: http://www.egeotraces.org.

References

Adly, C. L., J.-E. Tremblay, R. T. Powell, E. Armstrong, G. Peers, and N. M. Price (2015), Response of heterotrophic bacteria in a mesoscale iron enrichment in the northeast subarctic Pacific Ocean, *Limnology and Oceanography*, *60*(1), 136–148, doi: http://dx.doi.org/10.1002/lno.10013.

Boiteau, R. M., and D. J. Repeta (2015), An extended siderophore suite from Synechococcus sp. PCC 7002 revealed by LC-ICPMS-ESIMS, *Metallomics*, *7*(5), 877–884, doi: http://dx.doi.org/10.1039/C5MT00005J.

Boyd, P. W., and M. J. Ellwood (2010), The biogeochemical cycle of iron in the ocean, *Nature Geosci*, *3*(10), 675–682, doi:http://dx.doi.org/10.1038/ngeo964.

Boyle, E. A., R. F. Anderson, G. A. Cutter, R. Fine, W. J. Jenkins, and M. Saito (2015), Introduction to the U.S. GEOTRACES North Atlantic Transect (GA-03): USGT10 and USGT11 cruises, *Deep Sea Research Part II: Topical Studies in Oceanography*, *116*, 1–5, doi:https://doi.org/10.1016/j.dsr2.2015.02.031.

Browning, T. J., E. P. Achterberg, J. C. Yong, I. Rapp, C. Utermann, A. Engel, and C. M. Moore (2017), Iron limitation of microbial phosphorus acquisition in the tropical North Atlantic, *Nature Communications*, *8*, 15,465, doi:http://dx.doi.org/10.1038/ncomms15465.

Buck, K. N., B. Sohst, and P. N. Sedwick (2015), The organic complexation of dissolved iron along the U.S. GEOTRACES (GA03) North Atlantic Section, *Deep Sea Research Part II: Topical Studies in Oceanography*, *116*, 152–165, doi: http://dx.doi.org/10.1016/j.dsr2.2014.11.016.

Buck, K. N., P. N. Sedwick, B. Sohst, and C. A. Carlson (2018), Organic complexation of iron in the eastern tropical South Pacific: Results from US GEOTRACES Eastern Pacific Zonal Transect (GEOTRACES cruise GP16), *Marine Chemistry*, *201*, 229–241, doi: https://doi.org/10.1016/j.marchem.2017.11.007.

Conway, T. M., and S. G. John (2014), Quantification of dissolved iron sources to the North Atlantic Ocean, *Nature*, *511*(7508), 212–215, doi:http://dx.doi.org/10.1038/nature13482.

Conway, T. M., J. B. Palter, and G. F. de Souza (2018), Gulf Stream rings as a source of iron to the North Atlantic subtropical gyre, *Nature Geoscience*, doi: https://doi.org/10.1038/s41561-018-0162-0.

Deutsch, C., J. L. Sarmiento, D. M. Sigman, N. Gruber, and J. P. Dunne (2007), Spatial coupling of nitrogen inputs and losses in the ocean, *Nature*, *445*, 163, doi: http://dx.doi.org/10.1038/nature05392.

Fitzsimmons, J. N., G. G. Carrasco, J. Wu, S. Roshan, M. Hatta, C. I. Measures, T. M. Conway, S. G. John, and E. A. Boyle (2015), Partitioning of dissolved iron and iron isotopes into soluble and colloidal phases along the GA03 GEOTRACES North Atlantic Transect, *Deep Sea Research Part II: Topical Studies in Oceanography*, *116*, 130–151, doi: http://dx.doi.org/10.1016/j.dsr2.2014.11.014.

Galbraith, E. D., A. Gnanadesikan, J. P. Dunne, and M. R. Hiscock (2010), Regional impacts of iron-light colimitation in a global biogeochemical model, *Biogeosciences*, *7*(3), 1043–1064, doi:http://dx.doi.org/10.5194/bg-7-1043-2010.

Gent, P. R., and J. C. Mcwilliams (1990), Isopycnal mixing in ocean circulation models, *Journal of Physical Oceanography*, *20*(1), 150–155, doi:http://dx.doi.org/10.1175/1520-0485(1990)020<0150:imiocm>2.0.co;2.

Gerringa, L. J., M. J. Rijkenberg, J. Bown, A. R. Margolin, P. Laan, and H. J. W. De Baar (2016), Fe-binding dissolved organic ligands in the oxic and suboxic waters of the Black Sea, *Frontiers in Marine Science*, *3*, doi:http://dx.doi.org/10.3389/fmars.2016.00084.

Gerringa, L. J. A., M. J. A. Rijkenberg, V. Schoemann, P. Laan, and H. J. W. de Baar (2015), Organic complexation of iron in the West Atlantic Ocean, *Marine Chemistry*, *177, Part 3*, 434–446, doi:http://dx.doi.org/10.1016/j.marchem.2015.04.007.

Gledhill, M., and K. Buck (2012), The organic complexation of iron in the marine environment: A review, *Frontiers in Microbiology*, *3*(69), doi: http://dx.doi.org/10.3389/fmicb.2012.00069.

Hassler, C., C. van den Berg, and P. Boyd (2017), Towards a regional classification to provide a more inclusive examination of the ocean biogeochemistry of iron-binding ligands, *Frontiers in Marine Science*, *4*(19), doi:http://dx.doi.org/10.3389/fmars.2017.00019.

Hassler, C. S., V. Schoemann, C. M. Nichols, E. C. V. Butler, and P. W. Boyd (2011), Saccharides enhance iron bioavailability to Southern Ocean phytoplankton, *Proceedings of the National Academy of Sciences*, *108*(3), 1076–1081, doi: http://dx.doi.org/10.1073/pnas.1010963108.

Hatta, M., C. I. Measures, J. Wu, S. Roshan, J. N. Fitzsimmons, P. Sedwick, and P. Morton (2015), An overview of dissolved Fe and Mn distributions during the 2010-2011 U.S. GEOTRACES north Atlantic cruises: GEOTRACES GA03, *Deep Sea Research Part II: Topical Studies in Oceanography*, *116*, 117–129, doi: http://dx.doi.org/10.1016/j.dsr2.2014.07.005.

Honeyman, B. D., and P. H. Santschi (1989), A Brownian-pumping model for oceanic trace metal scavenging: Evidence from Th isotopes, *Journal of Marine Research*, *47*(4), 951–992, doi:http://dx.doi.org/10.1357/002224089785076091.

Hutchins, D. A., and P. W. Boyd (2016), Marine phytoplankton and the changing ocean iron cycle, *Nature Clim. Change*, *6*(12), 1072–1079, doi: http://dx.doi.org/10.1038/nclimate3147.

Ingall, E. D., J. M. Diaz, A. F. Longo, M. Oakes, L. Finney, S. Vogt, B. Lai, P. L. Yager, B. S. Twining, and J. A. Brandes (2013), Role of biogenic silica in the removal of iron from the Antarctic seas, *Nat Commun*, *4*, doi:http://dx.doi.org/10.1038/ncomms2981.

Laglera, L. M., and C. M. G. van den Berg (2009), Evidence for geochemical control of iron by humic substances in seawater, *Limnology and Oceanography*, *54*(2), 610–619, doi: http://dx.doi.org/10.4319/lo.2009.54.2.0610.

Large, W. G., J. C. McWilliams, and S. C. Doney (1994), Oceanic vertical mixing: A review and a model with a nonlocal boundary layer parameterization, *Reviews of Geophysics*, *32*(4), 363–403, doi:http://dx.doi.org/10.1029/94RG01872.

Macrellis, H. M., C. G. Trick, E. L. Rue, G. Smith, and K. W. Bruland (2001), Collection and detection of natural iron-binding ligands from seawater, *Marine Chemistry*, *76*(3), 175–187, doi:http://dx.doi.org/10.1016/S0304-4203(01)00061-5.

Marshall, J., A. Adcroft, C. Hill, L. Perelman, and C. Heisey (1997a), A finite-volume, incompressible navier stokes model for studies of the ocean on parallel computers, *Journal of Geophysical Research: Oceans*, *102*(C3), 5753–5766, doi: http://dx.doi.org/10.1029/96JC02775.

Marshall, J., C. Hill, L. Perelman, and A. Adcroft (1997b), Hydrostatic, quasi-hydrostatic, and nonhydrostatic ocean modeling, *Journal of Geophysical Research: Oceans*, *102*(C3), 5733–5752, doi:http://dx.doi.org/10.1029/96JC02776.

Mawji, E., R. Schlitzer, E. M. Dodas, C. Abadie, W. Abouchami, R. F. Anderson, O. Baars, K. Bakker, M. Baskaran, N. R. Bates, K. Bluhm, A. Bowie, J. Bown, M. Boye, E. A. Boyle, P. Branellec, K. W. Bruland, M. A. Brzezinski, E. Bucciarelli, K. Buesseler, E. Butler, P. Cai, D. Cardinal, K. Casciotti, J. Chaves, H. Cheng, F. Chever, T. M. Church, A. S. Colman, T. M. Conway, P. L. Croot, G. A. Cutter, H. J. W. de Baar, G. F. de Souza, F. Dehairs, F. Deng, H. T. Dieu, G. Dulaquais, Y. Echegoyen-Sanz, R. Lawrence Edwards, E. Fahrbach, J. Fitzsimmons, M. Fleisher, M. Frank, J. Friedrich, F. Fripiat, S. J. G. Galer, T. Gamo, E. G. Solsona, L. J. A. Gerringa, J. M. Godoy, S. Gonzalez, E. Grossteffan, M. Hatta, C. T. Hayes, M. I. Heller, G. Henderson, K.-F. Huang, C. Jeandel, W. J. Jenkins, S. John, T. C. Kenna, M. Klunder, S. Kretschmer, Y. Kumamoto, P. Laan, M. Labatut, F. Lacan, P. J. Lam, D. Lannuzel, F. le Moigne, O. J. Lechtenfeld, M. C. Lohan, Y. Lu, P. Masqué, C. R. McClain, C. Measures, R. Middag, J. Moffett, A. Navidad, J. Nishioka, A. Noble, H. Obata, D. C. Ohnemus, S. Owens, F. Planchon, C. Pradoux, V. Puigcorbé, P. Quay, A. Radic, M. Rehkämper, T. Remenyi, M. J. A. Rijkenberg, S. Rintoul, L. F. Robinson, T. Roeske, M. Rosenberg, M. R. van der Loeff, E. Ryabenko, M. A. Saito, et al. (2015), The GEOTRACES Intermediate Data Product 2014, *Marine Chemistry*, *177, Part 1*, 1–8, doi:http://dx.doi.org/10.1016/j.marchem.2015.04.005.

Moore, C. M., M. M. Mills, E. P. Achterberg, R. J. Geider, J. LaRoche, M. I. Lucas, E. L. McDonagh, X. Pan, A. J. Poulton, M. J. A. Rijkenberg, D. J. Suggett, S. J. Ussher, and E. M. S. Woodward (2009), Large-scale distribution of Atlantic nitrogen fixation controlled by iron availability, *Nature Geoscience*, *2*, 867, doi: http://dx.doi.org/10.1038/ngeo667.

Moore, C. M., M. M. Mills, K. R. Arrigo, I. Berman-Frank, L. Bopp, P. W. Boyd, E. D. Galbraith, R. J. Geider, C. Guieu, S. L. Jaccard, T. D. Jickells, J. La Roche, T. M. Lenton, N. M. Mahowald, E. Maranon, I. Marinov, J. K. Moore, T. Nakatsuka, A. Oschlies, M. A. Saito, T. F. Thingstad, A. Tsuda, and O. Ulloa (2013), Processes and patterns of oceanic nutrient limitation, *Nature Geosci*, *6*(9), 701–710, doi:http://dx.doi.org/10.1038/ngeo1765 http://www.nature.com/ngeo/journal/v6/n9/abs/ngeo1765.html-supplementary-information.

Moore, M. C., M. M. M, M. Angela, L. REBECCA, A. E. P., L. KARIN, G. R. J., and L. R. JULIE (2006), Iron limits primary productivity during spring bloom development in the central North Atlantic, *Global Change Biology*, *12*(4), 626–634, doi: http://dx.doi.org/10.1111/j.1365-2486.2006.01122.x.

Parekh, P., M. J. Follows, and E. A. Boyle (2005), Decoupling of iron and phosphate in the global ocean, *Global Biogeochemical Cycles*, *19*(2), GB2020, doi: http://dx.doi.org/10.1029/2004GB002280.

Pham, A. L. D., and T. Ito (2018), Formation and Maintenance of the GEOTRACES Subsurface-Dissolved Iron Maxima in an Ocean Biogeochemistry Model, *Global Biogeochemical Cycles*, *32*(6), 932–953, doi:http://dx.doi.org/10.1029/2017GB005852.

Redi, M. H. (1982), Oceanic isopycnal mixing by coordinate rotation, *Journal of Physical Oceanography*, *12*(10), 1154–1158, doi:http://dx.doi.org/10.1175/1520-0485(1982)012<1154:OIMBCR>2.0.CO;2.

Rijkenberg, M. J. A., R. Middag, P. Laan, L. J. A. Gerringa, H. M. van Aken, V. Schoemann, J. T. M. de Jong, and H. J. W. de Baar (2014), The Distribution of Dissolved Iron in the West Atlantic Ocean, *PLoS ONE*, *9*(6), e101,323, doi: http://dx.doi.org/10.1371/journal.pone.0101323.

Rue, E. L., and K. W. Bruland (1995), Complexation of iron(III) by natural organic ligands in the Central North Pacific as determined by a new competitive ligand equilibration/adsorptive cathodic stripping voltammetric method, *Marine Chemistry*, *50*(1), 117–138, doi:http://dx.doi.org/10.1016/0304-4203(95)00031-L.

Schlitzer, R., R. F. Anderson, E. M. Dodas, M. Lohan, W. Geibert, A. Tagliabue, A. Bowie, C. Jeandel, M. T. Maldonado, W. M. Landing, D. Cockwell, C. Abadie, W. Abouchami, E. P. Achterberg, A. Agather, A. Aguliar-Islas, H. M. van Aken, M. Andersen, C. Archer, M. Auro, H. J. de Baar, O. Baars, A. R. Baker, K. Bakker, C. Basak, M. Baskaran, N. R. Bates, D. Bauch, P. van Beek, M. K. Behrens, E. Black, K. Bluhm, L. Bopp, H. Bouman, K. Bowman, J. Bown, P. Boyd, M. Boye, E. A. Boyle, P. Branellec, L. Bridgestock, G. Brissebrat, T. Browning, K. W. Bruland, H.-J. Brumsack, M. Brzezinski, C. S. Buck, K. N. Buck, K. Buesseler, A. Bull, E. Butler, P. Cai, P. C. Mor, D. Cardinal, C. Carlson, G. Carrasco, N. Casacuberta, K. L. Casciotti, M. Castrillejo, E. Chamizo, R. Chance, M. A. Charette, J. E. Chaves, H. Cheng, F. Chever, M. Christl, T. M. Church, I. Closset, A. Colman, T. M. Conway, D. Cossa, P. Croot, J. T. Cullen, G. A. Cutter, C. Daniels, F. Dehairs, F. Deng, H. T. Dieu, B. Duggan, G. Dulaquais, C. Dumousseaud, Y. Echegoyen-Sanz, R. L. Edwards, M. Ellwood, E. Fahrbach, J. N. Fitzsimmons, A. Russell Flegal, M. Q. Fleisher, T. van de Flierdt, M. Frank, J. Friedrich, F. Fripiat, H. Fröllje, S. J. G. Galer, T. Gamo, R. S. Ganeshram, J. Garcia-Orellana, E. Garcia-Solsona, M. Gault-Ringold, E. George, et al. (2018), The GEOTRACES Intermediate Data Product 2017, *Chemical Geology*, doi:https://doi.org/10.1016/j.chemgeo.2018.05.040.

Solomon, H. (1971), On the representation of isentropic mixing in ocean circulation models, *Journal of Physical Oceanography*, *1*(3), 233–234, doi:http://dx.doi.org/10.1175/1520-0485(1971)001<0233:OTROIM>2.0.CO;2.

Tagliabue, A., O. Aumont, R. DeAth, J. P. Dunne, S. Dutkiewicz, E. Galbraith, K. Misumi, J. K. Moore, A. Ridgwell, E. Sherman, C. Stock, M. Vichi, C. Völker, and A. Yool (2016), How well do global ocean biogeochemistry models simulate dissolved iron distributions?, *Global Biogeochemical Cycles*, *30*(2), 149–174, doi: http://dx.doi.org/10.1002/2015GB005289.

Tagliabue, A., A. R. Bowie, P. W. Boyd, K. N. Buck, K. S. Johnson, and M. A. Saito (2017), The integral role of iron in ocean biogeochemistry, *Nature*, *543*(7643), 51–59, doi: http://dx.doi.org/10.1038/nature21058.

Twining, B. S., and S. B. Baines (2013), The trace metal composition of marine phytoplankton, *Annual Review of Marine Science*, *5*(1), 191–215, doi: http://dx.doi.org/10.1146/annurev-marine-121211-172322.

Twining, B. S., S. Rauschenberg, P. L. Morton, and S. Vogt (2015), Metal contents of phytoplankton and labile particulate material in the North Atlantic Ocean, *Progress in Oceanography*, *137*, 261–283, doi:https://doi.org/10.1016/j.pocean.2015.07.001.

Velasquez, I. B., E. Ibisanmi, E. W. Maas, P. W. Boyd, S. Nodder, and S. G. Sander (2016), Ferrioxamine siderophores detected amongst iron binding ligands produced during the remineralization of marine particles, *Frontiers in Marine Science*, *3*(172), doi:

http://dx.doi.org/10.3389/fmars.2016.00172.

Völker, C., and A. Tagliabue (2015), Modeling organic iron-binding ligands in a three-dimensional biogeochemical ocean model, *Marine Chemistry*, *173*, 67–77, doi: http://dx.doi.org/10.1016/j.marchem.2014.11.008.

Vraspir, J. M., and A. Butler (2009), Chemistry of marine ligands and siderophores, *Annual Review of Marine Science*, *1*(1), 43–63, doi: http://dx.doi.org/10.1146/annurev.marine.010908.163712.

Wunsch, C., and P. Heimbach (2007), Practical global oceanic state estimation, *Physica D*, *230*, 197–208, doi:https://doi.org/10.1016/j.physd.2006.09.040.

Ye, Y., and C. Völker (2017), On the Role of Dust-Deposited Lithogenic Particles for Iron Cycling in the Tropical and Subtropical Atlantic, *Global Biogeochemical Cycles*, *31*(10), 1543–1558, doi:http://dx.doi.org/10.1002/2017GB005663.

Ye, Y., T. Wagener, C. Völker, C. Guieu, and D. A. Wolf-Gladrow (2011), Dust deposition: iron source or sink? a case study, *Biogeosciences*, *8*(8), 2107–2124, doi: http://dx.doi.org/10.5194/bg-8-2107-2011.